Received: 5 February 2026 | Revised: 12 March 2026 | Accepted: 7 April 2026
DOI: 10.1002/ep.70475

ENVIRONMENTAL PROGRESS & SUSTAINABLE ENERGY

ORIGINAL RESEARCH

Remediation & Treatment

Optimizing nanoclay-enhanced membranes for oil rejection using response surface methodology

Ayse Gul[1] | Dilek Senol-Arslan[2] | Mesut Baris[3] | Pınar Boyraz[1] | Name Nur Alibaz[1]

[1]Department of Civil Engineering, Abdullah Gül University, Kayseri, Turkey
[2]Department of Engineering Science, Abdullah Gül University, Kayseri, Turkey
[3]Department of Civil Engineering, Istanbul Gelisim University, Istanbul, Turkey

Correspondence
Dilek Senol-Arslan, Department of Engineering Science, Abdullah Gül University, Kayseri, Turkey.
Email: dilek.senol@agu.edu.tr

Abstract

The efficient separation of waste oil from contaminated water is critical due to its challenges in environmental and industrial applications. This study investigated the production and optimization of polysulphone (PSF) membranes using two different types of clay (nanomer clay/CN and commercial nanoclay/NC). Response Surface Methodology (RSM) was applied to optimize the basic production parameters and nanoclay concentrations systematically to maximize oil rejection and permeability flow. The experimental results showed that NC and CN significantly increased the hydrophilicity, permeability, and fouling resistance of the membrane compared to pure PSF membranes. The contact angle significantly decreased from 64.34° (pristine PSF) to 36.23° (2% NC), indicating highly improved hydrophilicity. Consequently, the pure water flux increased from 177.2 L/m^2 h to a maximum of 248.6 L/m^2 h (1% NC). Furthermore, the modified membranes exhibited outstanding anti-fouling properties; the flux recovery ratio (FRR) improved from 88.09% to 96.20% (1% CN), while the decline ratio (DR) drastically dropped from 60.89% to 32.14%. The optimized condition for maximum removal efficiency using a modified quadratic model revealed that 2572 mg/L oil can be treated with a PSF membrane containing 2.0% CN to remove 98.271% of the oil. The model also suggests superiority of CN over NC with desirability factors of 0.978 and 0.900, respectively, while both demonstrated high efficiency. This theoretically modeled experimental comparative study highlights the importance of PSF membrane technology for efficient and sustainable oil–water separation and demonstrates the promising potential of nanoclay modifications.

KEYWORDS
nanoclay, oil rejection, PSF membrane, RSM, water treatment

1 | INTRODUCTION

Rapid industrial production and human activity growth have significantly increased the discharge of oily wastewater from sectors such as petroleum, chemical, food processing, and metal industries.[1] Containing various pollutants, oily wastewater poses serious risks to water resources, aquatic ecosystems, and human health if not adequately treated.[2] Ecological impacts such as oil spills and the continuous release of hazardous effluents threaten environmental quality. Additionally, oily pollution is a complex contaminant in aquatic environments.[3] Notably, a single liter of waste vegetable oil can contaminate up to one million liters of drinking water.[4] Consequently, water pollution caused by these discharges has become a critical environmental concern, especially given the persistence and widespread presence of oily wastewater in water bodies.[5] Increasing global water demand, limited water resources, and the impacts of climate change further emphasize the need for effective treatment methods, pollution prevention at the source, and water conservation to ensure environmental sustainability and protect the balance for future generations.

Various treatment techniques have been studied for the removal of emulsified oils from water, including microfiltration,[6] ultrafiltration,[7] pervaporation,[8] electrocoagulation,[9] and reverse osmosis.[10] Among these methods, adsorption and membrane separation are particularly favored due to their high efficiency and low energy consumption. Membrane technology has emerged as a promising and sustainable solution for oily wastewater treatment, offering not only cost-effectiveness and high separation efficiency but also minimal secondary pollution and ease of recycling.[11] Adopting membrane-based processes is increasingly recognized as a viable approach for effective oil–water separation, which supports global efforts to mitigate water pollution and promote water conservation in the face of growing environmental challenges.

Polymeric membranes, especially those incorporated with TiO_2,[12] SiO_2,[1] cellulose,[13] silica,[14] and clay nanoparticles,[15] are commonly used for oily wastewater treatment. Polymeric membranes play a crucial role in oily wastewater treatment due to their enhanced hydrophilicity, antifouling properties, and high separation efficiency, enabling more sustainable and effective removal of oil contaminants from water.[16]

Among various nanoparticles explored for membrane enhancement, organically modified montmorillonite nanoclays have emerged as particularly promising additives, including materials such as Nanomer I.44P, modified with dimethyldialkyl amines, and Nanomer I.31PS, which contains octadecylamine and aminopropyltriethoxysilane. Strong compatibility with polymer matrices supplies usability to them in membranes to increase hydrophilicity, porosity, and surface roughness. These improvements contribute to higher water flux, better fouling resistance during filtration, and increased removal efficiency.[17]

Aljlil developed a membrane composed of red clay and nano-activated carbon to treat industrial wastewater, reaching up to 99.96% oil removal efficiency at 80 NTU oil concentration under a pressure of 5 bar.[18] Nandi et al. prepared a ceramic microfiltration (MF) membrane from a clay mixture and achieved 97% oil removal at an oil concentration of 50 mg/L Nandi et al.[19] Vasanth et al. achieved 87% oil removal using cross-flow microfiltration with clay-based ceramic membranes.[20] Aloulou et al. developed a composite membrane incorporating TiO_2 and nanoclay materials for oily wastewater treatment, achieving a 99% oil removal efficiency.[21]

Recent research in oily wastewater remediation has increasingly prioritized the development of sustainable and cost-efficient membrane systems.[3] A notable example is the use of green additives, such as banana peel nanoparticles, which have been shown to enhance membrane hydrophilicity and achieve oil rejection rates of approximately 95.2%.[3] While these eco-friendly modifications are promising, their application to high-load, real-world waste oil streams remains limited, particularly regarding robust statistical optimization and economic scalability.

In this study, two types of clay-based membranes (PSF/NC and PSF/CN) were fabricated using different amounts (0.5%–2%) of nanoclay and nanomer to treat waste vegetable oil in water. These membranes were evaluated for oil removal efficiency, water flux, and fouling resistance under oily wastewater conditions. Statistical analysis using Design-Expert software and a Response Surface D-Optimal Design approach was performed to systematically examine the effects of oil concentration and nanoparticle content and optimize membrane performance. The results showed that the membranes achieved high oil removal rates, up to 98.6%, while maintaining stable water flux.

1.1 | Statement of novelty

The RSM analysis identified the best conditions for maximum oil removal using the membranes. By combining membrane preparation with statistical optimization, this study aims to provide a practical and effective approach for oil–water separation, supporting water conservation and environmental protection. Recent advancements in the field strongly emphasize the transition toward sustainable, eco-friendly, and cost-effective membrane technologies for oily wastewater treatment.[3] In this context, this study contributes to the literature by using real waste vegetable oil to compare unmodified and surface-modified nanoclays, unlike most studies that rely on synthetic emulsions. This approach ensures high reliability by demonstrating robust stability and high flux recovery against complex, un-pretreated real effluents. Moreover, the findings obtained from this study are of great importance for industrial sectors dealing with oily wastewater, such as petroleum refining, petrochemical processing, and food production processes. Membranes reinforced with optimized nanoclay have shown improvement in oil rejection efficiency. In terms of performance, the modified membranes achieved an outstanding oil removal efficiency of up to 98.27% under optimal conditions, which compares highly favorably with recent green-additive studies—such as the 95.2% rejection achieved using biological banana peel nanoparticles[3]—demonstrating the superior potential of organically modified nanoclays.

The use of natural, inexpensive, and environmentally friendly clay can lead to reduced treatment costs and increased compliance with environmental discharge regulations, directly improving the overall cost-efficiency of the process. The use of the RSM has provided an industry-friendly optimization framework that minimizes experimental costs and time and facilitates scale-up and process integration. Furthermore, since clay, which is abundant in nature, is an easily obtainable and low-cost additive, it supports the development of economically viable and sustainable membrane-based separation technologies for large-scale industrial applications.

From an environmental science perspective, the persistent nature of oily wastewater poses a severe threat to aquatic ecosystems, where even a single liter of waste vegetable oil can sustainably contaminate up to one million liters of drinking water.[4] This research contributes to pollution research by developing a low-energy, highly efficient membrane filtration approach that utilizes natural, abundant, and environmentally friendly clay nanoparticles rather than toxic or expensive synthetic modifiers. The potential implications for real-world applications are highly significant. By validating the membranes using real industrial effluents (waste vegetable oil from dining facilities) rather than synthetic emulsions, and successfully treating heavy-duty oil loads (up to 3000 mg/L with over 98% rejection) and an outstanding flux recovery ratio (FRR >96%), this approach proves its practical viability. The robust fouling resistance ensures that fouling is predominantly reversible, which offers industries a cost-effective strategy to extend membrane operational lifespan, minimize chemical cleaning requirements, and support large-scale sustainable wastewater management.

2 | MATERIALS AND METHODS

2.1 | Materials

PSF (with an average $M_w = 60{,}000$ Da) was supplied from Acros Organics (Geel, Belgium), DMF (N,N-Dimethylformamide) was obtained from Merck (Darmstadt, Germany). Nanoclay, Nanomer (I.44P, montmorillonite clay surface modified with 35–45 wt % dimethyldialkyl(C14-C18)amine), and Nanoclay surface modified (I.31PS contains 15–35 wt % octadecylamine, 0.5–5 wt % aminopropyltriethoxyslane) were purchased from Sigma-Aldrich (USA). Waste vegetable oil was collected from the university dining services on campus.

2.2 | Methods

2.2.1 | Membrane fabrication

The dope solution was prepared by first dispersing CN and NC nanoparticles in the solvent DMF through stirring. Once the nanoparticles were well mixed, the PSF polymer was slowly added to the suspension and stirred continuously until fully dissolved. The mixture was then sonicated to ensure an even distribution of the nanoparticles throughout the solution. Figure 1 provides a schematic overview of the fabrication process for the PSF membranes containing CN and NC nanoparticles. Detailed information on the components and their proportions in the dope solution is listed in Table 1.

TABLE 1 The components of the dope solution for PSF/CN and PSF/NC membranes.

	PSF (wt %)	NC (wt %)	DMF (wt %)
Membrane 1	15	-	85
	15	0.5	84.5
	15	1	84
	15	2	83
	PSF (wt %)	CN (wt %)	DMF (wt %)
Membrane 2	15	-	85
	15	0.5	84.5
	15	1	84
	15	2	83

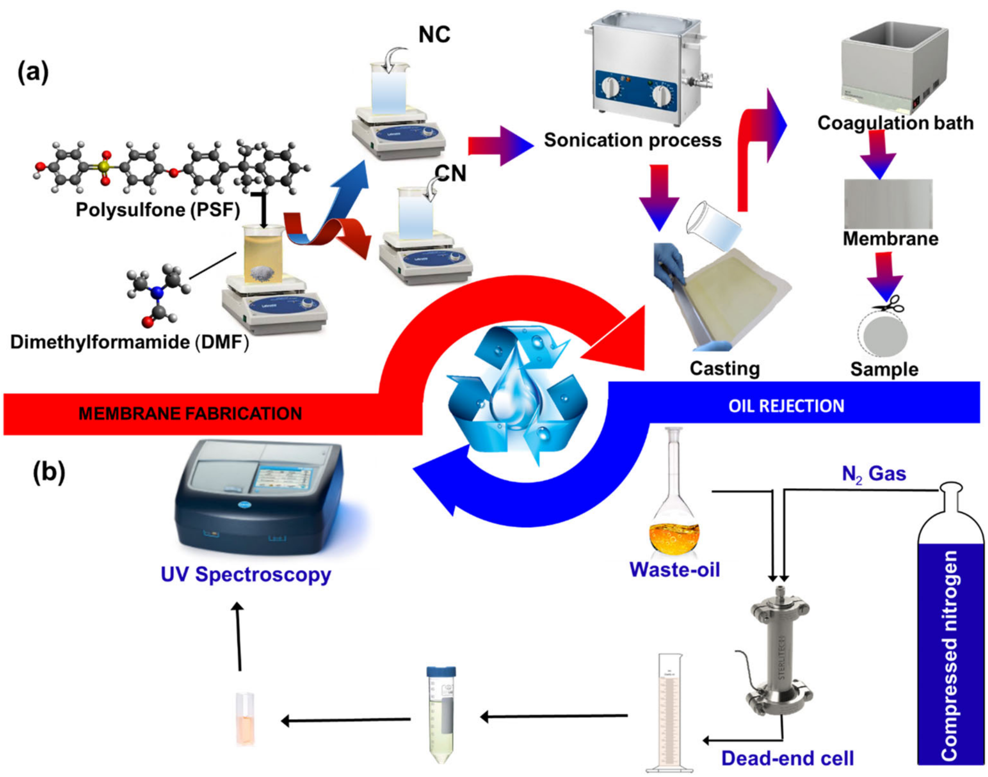

FIGURE 1 Schematic illustration of (a) Membrane fabrication (b) oil rejection experiments.

2.2.2 | Preparation of oil-in-water emulsions

A solution with a concentration of between 500 and 3000 g/L was created to establish an oil-in-water emulsion model. A homogeneous solution was obtained by mixing waste vegetable oil and distilled water for 1 h to make the oil-in-water emulsion model. A Hach UV–visible spectrophotometer set to 387 nm was used to measure the amount of oil in the permeate. The absorbance of the fluid being tested can be converted to determine the oil concentration value.

The emulsions were prepared using real WVO (waste vegetable oil) to represent actual food industry conditions. It is important to note that WVO contains free fatty acids and polar compounds formed during high-temperature frying, which act as natural stabilizers.[22] This approach provides a more realistic assessment of membrane performance than synthetic emulsions stabilized with commercial surfactants like SDS or CTAB, as real waste matrices involve complex interactions between diverse organic components.[23]

2.2.3 | Measurement of oil separation efficiency

The basic separation performance of the PSF, PSF/nanoclay, and PSF/nanomer membranes was evaluated using a dead-end stirred cell filtration system (Sterlitech, HP4750) with an effective membrane area of 14.6 cm^2 and a 300 mL-capacity filtration cell connected to a nitrogen gas cylinder for pressurization. Deionized water was used as the feed solution for the water flux tests, conducted at transmembrane pressures (TMP) of 5 bar, with a stirring speed of 250 rpm, and maintained at 25°C. The water fluxes of the membranes were calculated using Equation (1).

The oil rejection experiments were conducted in the same dead-end stirred cell filtration system at stirring speeds of 250 rpm under TMP conditions of 5 bar. Before the emulsion filtration tests, the membranes were preconditioned by filtering pure water for 15 min at 2 bar. Subsequently, 250 mL of the synthetic emulsion was filtered through the membranes. The separation flux (J), rejection ratio (RR), flux decay ratio (DR), and flux recovery ratio (FRR) were determined using Equations (1), (2), (3), and (4), respectively. The oil concentration in the treated samples was analyzed using UV–visible spectroscopy at 387 nm to evaluate the membranes' oil removal performance.

$$J = \frac{V}{Axt} \quad (1)$$

$$\%RR = \frac{C_0 - C}{C_0} \times 100 \quad (2)$$

$$DR = \frac{J - J_1}{J} \times 100 \quad (3)$$

$$FRR = \frac{J_2}{J} \times 100 \quad (4)$$

The water flux (J, L/m^2 h) was calculated using Equation (1), where $\boldsymbol{V}$ is the volume of permeate (L), $\boldsymbol{A}$ is the effective membrane area (m^2), and $\boldsymbol{t}$ is the filtration time (h). The oil rejection efficiency was determined based on the initial ($\boldsymbol{C_0}$, g/L) and final ($\boldsymbol{C}$, g/L) oil concentrations in the emulsion before and after filtration, respectively. The oil/water emulsion flux is denoted as $\boldsymbol{J_1}$ (L/m^2 h), while $\boldsymbol{J_2}$ (L/m^2 h) represents the water flux of the cleaned membrane after fouling and cleaning procedures. For the regeneration procedure, the fouled membranes were simply rinsed thoroughly with deionized water for 15 min to remove reversible foulants before measuring $\boldsymbol{J_2}$.

2.2.4 | Experimental design

In this study, a Response Surface Methodology (RSM) using the D-Optimal design was employed to efficiently investigate the effects of two numeric factors, nanoparticle percentage and feed oil concentration, alongside one categorical factor, nanomaterial type, on the system's performance, specifically the oil removal efficiency (Table 2). The D-Optimal design was selected due to its flexibility in handling quantitative and qualitative variables and its suitability for irregular experimental regions where classical factorial or central composite designs are impractical. This approach allows for constructing a statistically efficient model with minimal experimental runs, ensuring precise estimation of interaction effects and higher-order terms while optimizing resource use in laboratory experimentation. The adopted experiment design was Response Surface D-Optimal Design. The experiment runs included 23 runs.

2.3 | Characterization

2.3.1 | Contact angle measurements

The sessile drop method was used to measure the water contact angle to determine the changes in surface hydrophilicity of each of the PSF/NC and PSF/CN membrane after the addition of NC and CN Nps. The measurements were performed using Attention-Theta Lite, BiolinScientific, Finland.

2.3.2 | Fourier transform infrared spectrophotometer (FT-IR) measurements

FT-IR spectrometer (Thermo Nicolet Avatar 370) was used to identify the functional groups present in pure PSF, CN, and NC Nps, as well as in WVO and NC and CN embedded PSF membranes.

2.3.3 | Scanning electron microscopy (SEM)

The structure and morphology of NC and CN Nps and NC and CN embedded nanocomposite PSF membranes at three different ratios (2%, 1%, and 0.5%) were examined using a scanning electron microscope (Zeiss Gemini) with a 10 kV applied voltage.

TABLE 2 Implemented design build information and the factors levels.

File version		11.0.3.0					
Study type		Response surface				Subtype	Randomized
Design type		D-optimal		Coordinate Exchange		Runs	23
Design model		Reduced Cubic				Blocks	No Blocks
Build time (ms)		109.00					
Factor	**Name**	**Units**	**Type**	**Minimum**	**Maximum**	**Coded low**	**Coded high**
A	Oil Conc.	mg/L	NuCNic	500.	3000	−1 ↔ 500	+1 ↔ 3000
B	NanoP	%	NuCNic	0.0	2.0	−1 ↔ 0.00	+1 ↔ 2.00
C	Material		Categoric	NC	CN		

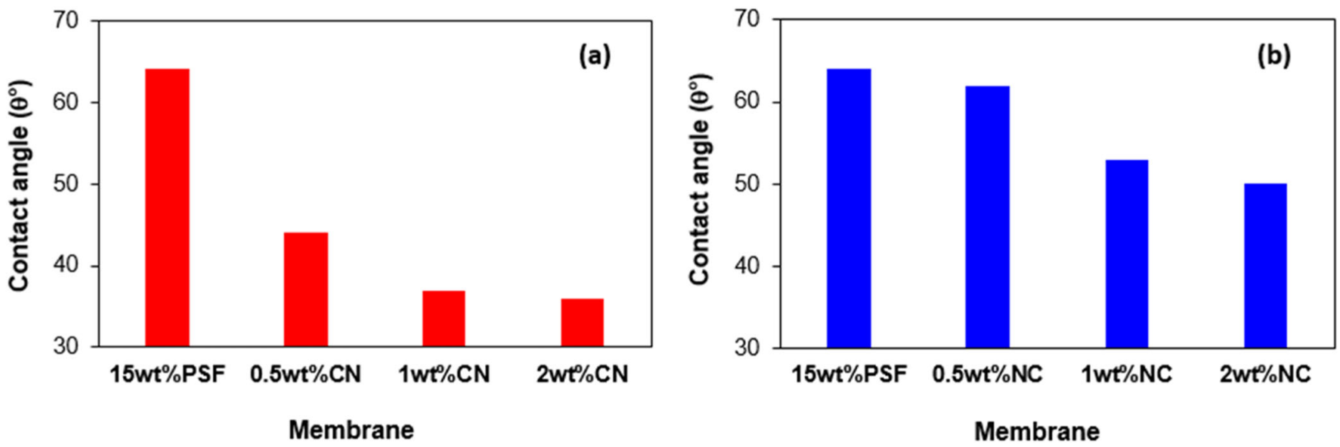

FIGURE 2 Contact angle measurements of (a) 15 wt % PSF, 0.5 wt % CN, 1 wt % CN, and 2 wt % CN embedded PSF membrane surfaces (b) 15 wt % PSF, 0.5 wt % NC, 1 wt% NC, and 2 wt% NC embedded PSF membrane surfaces.

3 | RESULTS AND DISCUSSION

3.1 | Characterization analysis of the membranes

3.1.1 | Contact angle

In this study, integrating CN and NC additives into PSF membranes markedly enhanced membrane hydrophilicity, as evidenced by the observed reduction in contact angle values. Specifically, the contact angle for membranes modified with CN declined from 64.34° for pristine PSF to 62.36°, 53.61°, and 50.28% upon incorporating 0.5%, 1%, and 2% CN, respectively. This trend indicates that increasing the nanomer concentration leads to enhanced surface wettability, likely due to the migration of hydrophilic groups toward the membrane surface and the increase in surface roughness. The presence of hydroxyl functionalities, high porosity, and the inherently hydrophilic nature of clay-based nanoparticles also contribute to this behavior.[24] Figure 2 presents the contact angle measurements of PSF/nanoclay and PSF/nanomer membranes.

A more substantial decrease in contact angle was achieved with the addition of NC, where CA values decreased from 64.34° (pristine PSF) to 44.34°, 37.05°, and 36.23% with the incorporation of 0.5%, 1%, and 2% NC, respectively. This sharper reduction demonstrates the superior capability of NC compared to CN in improving membrane hydrophilicity. This can be attributed to the intrinsic hydrophilic nature of NC and its uniform dispersion within the PSF matrix, which facilitates the exposure of hydrophilic sites on the membrane surface.[25]

The significant reduction in contact angle upon NC addition is expected to enhance water permeability and mitigate fouling during filtration processes, which is advantageous for practical water treatment applications. Similar improvements in membrane hydrophilicity upon incorporating nanofillers have been reported in previous studies, supporting the trends observed in the present work.[26,27]

These results demonstrate that incorporating hydrophilic CN and NC additives into PSF membranes effectively enhances surface wettability, with NC exhibiting a more pronounced effect. This improvement in hydrophilicity is beneficial for applications requiring high water affinity and fouling resistance, confirming the potential of these modifications in advancing membrane performance for water treatment.

These enhanced hydrophilic properties directly verify the novel anti-fouling observations detailed in the filtration sections. The significant reduction in contact angles structurally explains why the modified membranes demonstrated exceptionally high Flux Recovery Ratios (FRR up to 96.20%) and low Decline Ratios (DR) against complex, real waste vegetable oil without severe pore blockage.

3.1.2 | FTIR results

Fourier transform infrared (FTIR) spectroscopy is a powerful and widely applied technique for identifying functional groups and monitoring structural changes in polymeric membranes. The FTIR measurements of PSF/nanoclay and PSF/nanomer membranes are shown in Figure 3.

As shown in Figures (a) and (b), the FTIR spectra of pristine PSF, 1 wt % NC, and 1 wt % CN embedded PSF membranes, and after WVO removal with these membranes, provide a comprehensive representation of the infrared properties of the material.

The FTIR spectra of WVO showed characteristic C—H stretching bands at 2847–2960 cm^{-1}. The peak at 1430 cm^{-1} is attributed to the vibration of CH_2.[28] The peaks at 3522 and at 1593 cm^{-1} are for OH and COOH groups, respectively.[29]

The FTIR spectra of pristine PSF membrane exhibited peaks at 1243 cm^{-1}, 1587 cm^{-1}, which can be attributed to asymmetric stretching of C—H and C═C.[1,30]

The presence and integration of these functional groups confirm the chemical basis of the membrane modifications, directly supporting the physical mechanism behind the enhanced water affinity and the successful repulsion of hydrophobic WVO droplets.

3.1.3 | SEM results

SEM was used to examine the surface and cross-sectional morphology of the membranes. Figure 4 highlights structural differences in the pristine PSF, PSF/NC, and PSF/CN membranes.

Cross-sectional SEM images showed a distinct asymmetric structure consisting of a dense upper layer. The morphological characteristics of NC and CN NPs are distinctly different, as seen in Figures (b) and (c). NC particles appear irregular and clustered with relatively rough surfaces, while CN particles exhibit a flaky, layer-like structure and a long, finger-like solid substructure extending toward the membrane base.[31]

NC particles appear as irregular and aggregated clusters with relatively rough surfaces, while CN particles exhibit a more exfoliated, sheet-like structure. The latter indicates better dispersion potential due to organic surface modification, which improves interfacial compatibility with the PSF matrix.[32]

The exfoliated, sheet-like morphology and enhanced interfacial compatibility of the organically modified CN provide a structural basis for the observed performance improvements. This uniform dispersion within the PSF matrix minimizes macroscopic defects, which rationalizes why the PSF/CN membranes achieved a high desirability factor of 0.978 and an oil rejection of 98.27% under high-load WVO filtration conditions.

3.2 | Membrane filtration

Membrane fluxes were measured to evaluate their separation performance. Pure water, oily water, and cleaned membrane fluxes of PSF, PSF/NC, and PSF/CN membranes are shown in Figure 5.

The pristine PSF membrane exhibited a pure water flux of 177.2 L/m^2 h, which decreased to 69.3 L/m^2 h during oily wastewater filtration due to fouling. A high FRR of 96.19% indicated improved hydrophilicity and fouling resistance. Adding 1% nanomer increased pure water flux to 210.6 L/m^2 h and oily water flux to 136.2 L/m^2 h. At 2% nanomer loading, flux slightly decreased (198.7 L/m^2 h pure water, 132.3 L/m^2 h oily water), while a high FRR (93.44%) was maintained, showing that increased nanoparticle content sustained the membrane's performance.

Similarly, incorporating 1% nanoclay achieved the highest pure water flux (248.6 L/m^2 h) and oily water flux (155.4 L/m^2 h), with a

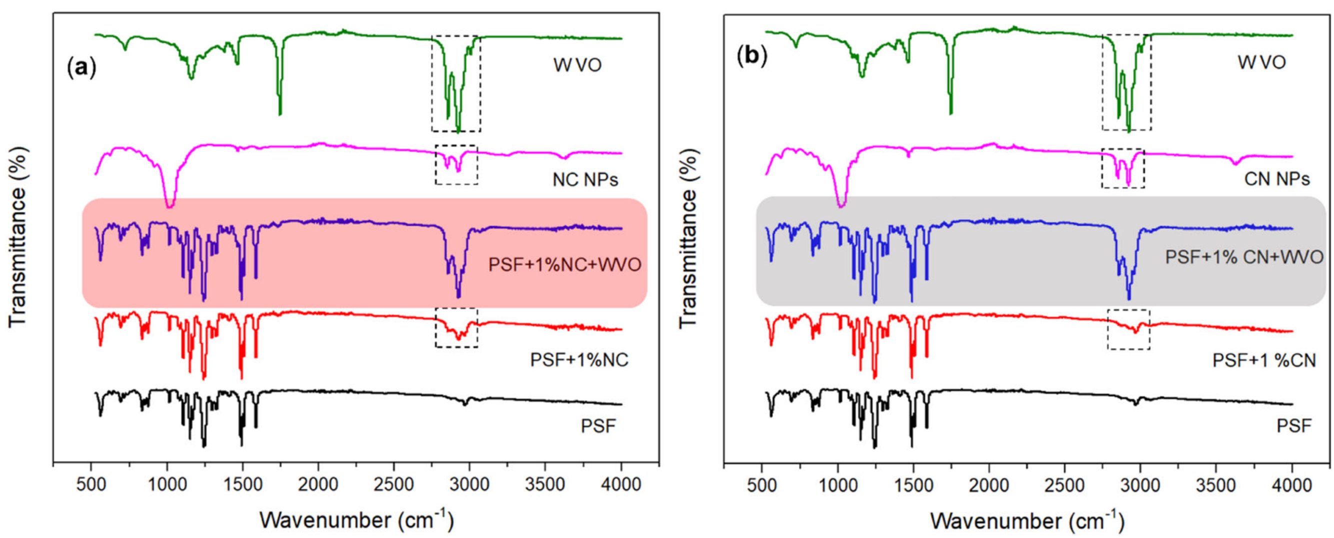

FIGURE 3 (a) The FTIR spectra of WVO, NC NPs, PSF + 1 wt % NC + WVO, PSF + 1 wt % NC, and PSF. (b) WVO, CN NPs, PSF + 1 wt % CN + WVO, PSF + 1 wt % CN, and PSF.

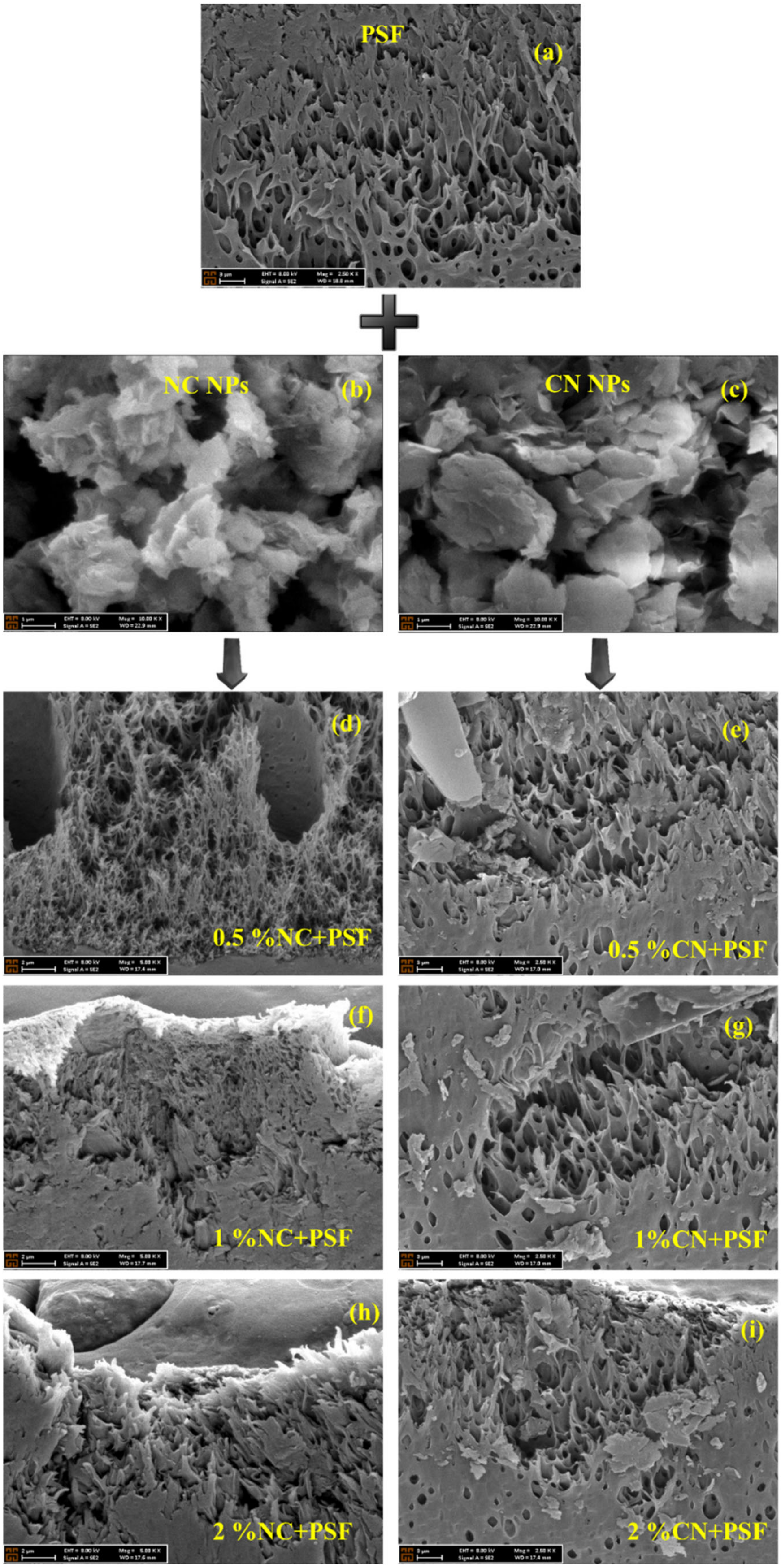

FIGURE 4 The cross-section SEM images of (a) pristine PSF membrane, (b) NC NPs, (c) CN NPs, (d, f, and h) morphology of modified PSF membranes with different NC NPs at 0.5%, 1%, and 2% concentrations (e, g, and i) morphology of modified PSF membranes with different CN NPs at 0.5%, 1%, and 2% concentrations.

high FRR (94.61%) and superior enhancement over nanomer-modified membranes. At 2% nanoclay, flux slightly decreased (239.3 L/m^2 h pure water, 138.5 L/m^2 h oily water), but the FRR (89.88%) remained acceptable.

The significant enhancement in both pure and oily water fluxes upon the incorporation of CN and NC nanoparticles can be attributed to several underlying mechanisms. Primarily, as evidenced by the contact angle measurements, the intrinsic hydrophilic nature of the clay nanoparticles substantially increases the surface wettability of the modified membranes. This enhanced hydrophilicity facilitates the rapid adsorption and transport of water molecules through the membrane matrix while effectively repelling hydrophobic oil droplets, thereby reducing overall water transport resistance. Furthermore, the integration of these nanofillers modifies the internal microstructure of the membrane, increasing the overall porosity and creating additional pathways for water permeation, which collectively contribute to the observed flux improvements.

Statistical analysis (reduced cubic model, Adjusted $R^2 = 0.9471$; Predicted $R^2 = 0.8919$) confirmed that oil concentration, nanoparticle percentage, and their interactions significantly affected performance ($p < 0.05$). Optimization showed that high nanoparticle loading (2%) at high oil concentrations (~2500 mg/L) achieved high desirability (~0.978), demonstrating that modified membranes can efficiently handle high-load oily wastewater while maintaining enhanced flux and antifouling properties.

Furthermore, to clearly demonstrate the impact of membrane modification on separation performance, Figure 6 compares the oil rejection efficiencies of the unmodified (0%) and modified (2%) NC and CN membranes under both low (500 mg/L) and severe (3000 mg/L) initial oil loads. The clustered bar chart clearly visualizes that under a heavy oil load, the 0% clay membranes exhibit limited efficiency, whereas the incorporation of 2% nanoclay significantly sustains and enhances the separation performance, reaching an outstanding 98.61% rejection for the 2% CN-modified membrane at 3000 mg/L.

While this study successfully utilized real waste vegetable oil to simulate the organic phase of food industry effluents, distilled water was used as the continuous phase to establish a controlled baseline for membrane evaluation. In practical applications, however,

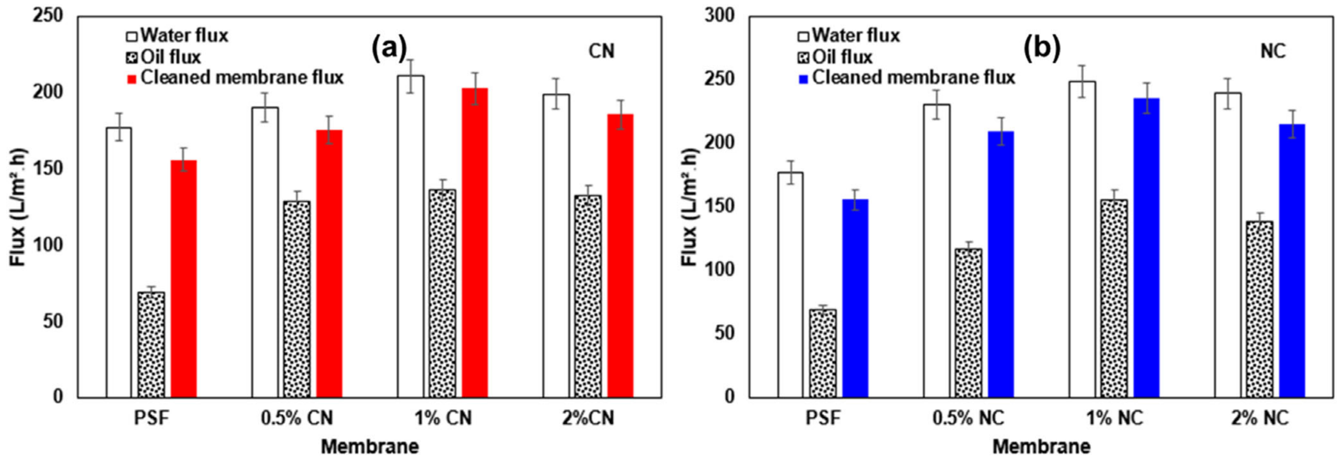

FIGURE 5 (a) Pure water, oily water, and cleaned membrane fluxes of 15 wt% PSF and three different concentrations of CN (0.5, 1, and 2). (b) Pure water, oily water, and cleaned membrane fluxes of 15 wt% PSF and three different concentrations of NC (0.5, 1, and 2).

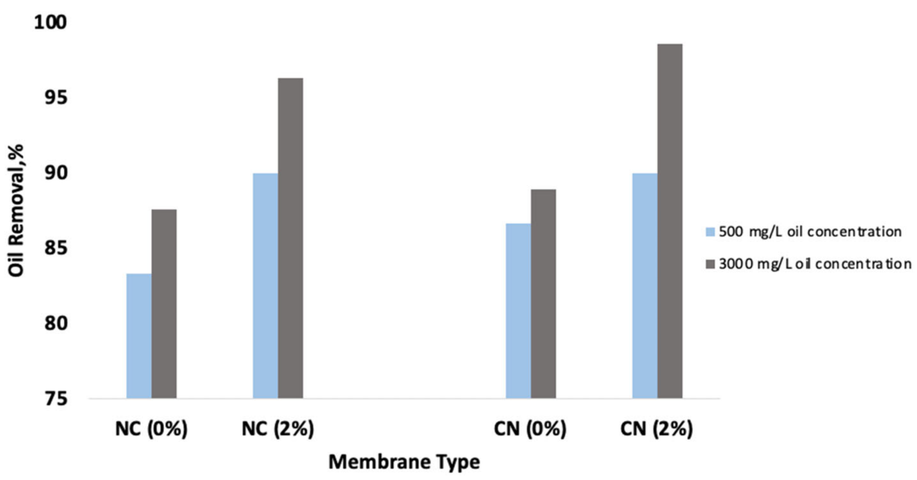

FIGURE 6 Comparative oil rejection efficiencies of the unmodified (0%) and modified (2%) NC and CN membranes at the lowest (500 mg/L) and highest (3000 mg/L) tested initial oil concentrations.

wastewater matrices are significantly more complex, containing dissolved ions and salts that can compress the electrical double layer of both the oil droplets and the membrane surface. This phenomenon can destabilize emulsions and accelerate fouling. Since typical polymeric ultrafiltration membranes are effective at rejecting oil but generally allow dissolved ions to pass through,[23] holistic treatment of such streams may require integrated processes. Consequently, investigating the impact of varying ionic strengths on the separation efficiency and long-term durability of these nanoclay-enhanced membranes represents a vital direction for future research.

The high oil rejection and antifouling success of the modified membranes are primarily due to the formation of a stable water layer on the surface. During the membrane preparation process, the hydrophilic clay nanoparticles (NC and CN) migrate toward the surface and pore walls.[33,34] These clay sites then attract water molecules to create a protective hydration layer across the membrane interface.[35,36] This layer not only helps water pass through more easily, increasing the flux, but also acts as a physical barrier against oil. Since waste vegetable oil is hydrophobic, it is repelled by this water layer and cannot stick to the membrane surface or block the pores. This mechanism explains why our modified membranes reached over 98% oil rejection and showed excellent flux recovery (FRR) results.[37]

3.3 | Fouling resistance of the membrane

The FRR and DR values of the PSF/nanoclay, and PSF/nanomer membranes obtained for waste vegetable oil at 5 bar were presented in Figure 7.

The figure 7 presents the Flux Recovery Ratio (FRR) and Decline Ratio (DR) values for pristine PSF membranes and PSF membranes modified with varying concentrations of CN and NC. It can be observed that DR values ranged from 32.14% to 60.89%. In comparison, FRR values varied between 88.09% and 96.20% during waste vegetable oil wastewater treatment, highlighting the influence of nanoparticle incorporation on membrane performance.

In this study, it is essential to note that DR does not represent oil rejection; rather, it denotes the reduction in water flux resulting from fouling during wastewater filtration with waste vegetable oil. Higher DR values indicate a greater decline in flux due to fouling, whereas lower DR values reflect reduced flux decline during operation, signifying improved fouling resistance.

The pristine PSF membrane demonstrated an FRR of 88.09% alongside a DR of 60.89%. Following the incorporation of CN, a notable increase in FRR was observed with rising CN concentrations, achieving a maximum FRR of 96.20% at a 1% CN loading. However, a slight decrease to 93.46% was recorded at 2% CN, which may be attributed to nanoparticle agglomeration at higher loadings, potentially leading to partial pore blockage or structural alterations within the membrane matrix. Concurrently, DR values decreased significantly with CN incorporation, reaching 32.14% at 0.5% CN and maintaining values in the 33%–35% range at higher concentrations. This indicates reduced flux decline and enhanced fouling resistance upon CN addition.

For membranes modified with NC, improvements in FRR were similarly evident compared to the pristine PSF membrane, with the highest FRR of 94.61% achieved at 1% NC loading. A decrease in FRR was noted at 2% NC, suggesting a similar trend of potential nanoparticle aggregation or pore structure modifications at elevated concentrations. Although the incorporation of NC also reduced DR, the decrease was less pronounced than that observed with CN, with DR values declining from 49.31% at 0.5% NC to 42.12% at 2% NC loading.

A high FRR typically indicates that fouling can be effectively removed from the membrane surface through cleaning, suggesting predominantly reversible fouling behavior.[38] Therefore, incorporating CN and NC into PSF membranes increased FRR values, reflecting improved fouling resistance and enhanced cleaning efficiency. Simultaneously, the reduction in DR values demonstrates a decrease in flux decline during waste vegetable oil wastewater treatment. The most favorable performance in terms of fouling resistance was observed at a 1% loading for CN and NC. At the same time, higher nanoparticle

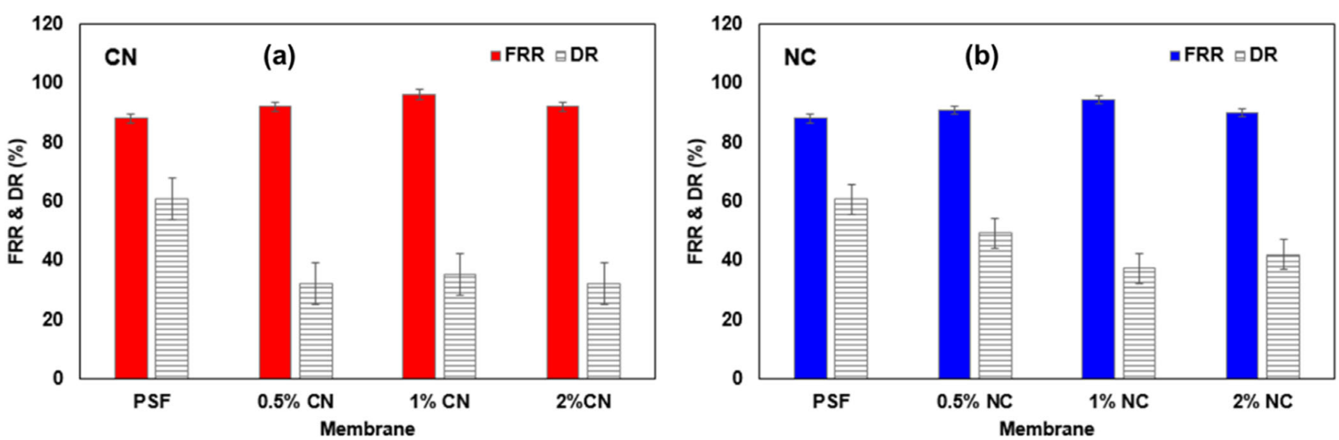

FIGURE 7 FRR and DR of membranes at 5 bar during waste vegetable oil wastewater treatment.

concentrations resulted in slight reductions in FRR, likely due to nanoparticle aggregation within the membrane structure.

Previous studies have reported that cellulose nanomaterials and clay-based nanoparticles exhibit good dispersion within the polymer matrix at lower concentrations. However, as the concentration of clay increases beyond 3 wt %, partial accumulation of nanoparticles on the membrane surface has been observed, which may affect membrane morphology and fouling behavior.[24]

3.4 | Final equation in terms of coded and actual factors

The predictive equation of the model can be expressed in terms of the actual variables within their initially adjusted ranges. Since these variables are not normalized, the coefficients are determined based on the units of each specific variable; therefore, they should not be used to assess the relative impact of the variables. Experimental responses are presented in Table 3.

On the other hand, an equation with coded factors is used to assess the relative impact of different variables. Generally, these coded factors range from −1 (lowest level) to +1 (highest level).

TABLE 3 The obtained experimental responses.

Run	Oil Conc. (mg/L) A	NanoP (%) B	Material C	Oil Remov. (%)
1A	2750	1	CN	91.6
2	1750	2	NC	96.6
3	3000	2	CN	98.61
4	500	2	NC	90
5	3000	0	CN	88.9
6	3000	2	CN	98.61
7	1750	2	CN	95.92
8	500	2	NC	86.67
9	500	0	CN	86.67
10	3000	2	NC	96.3
11	500	1	NC	85.7
12	500	1	CN	86.67
13	500	0	NC	83.33
14	1750	0.5	CN	93.88
~~15~~	~~3000~~	~~0.5~~	~~NC~~	~~95.83~~
16	3000	0	NC	87.6
~~17~~	~~1625~~	~~1~~	~~CN~~	~~85~~
18	1531	1	NC	93.33
19	3000	2	NC	96.3
20	2125	0	NC	92.21
21	500	2	CN	90
22	1750	0	CN	95.23
23	2500	1.5	NC	95.6

$$\text{Oil Remov} = +93.76 + 2.76\,A + 1.22\,B - 0.1682\,C + 1.29\,AB - 0.2124\,AC - 0.2609\,BC - 5.06\,A^2 + 1.28\,B^2 + 2.14\,A^2B + 1.17\,B^2C$$

Material: NC

$$\text{Oil Remov.} = +76.08534 + 0.017469\,\text{Oil Conc.} + 3.66388\,\text{NanoP} - 0.003761\,\text{Oil Conc.} * \text{NanoP} - 4.60551\text{E-06}\,\text{Oil Conc.}^2 + 0.104996\,\text{NanoP}^2 + 1.36887\text{E-06}\,\text{Oil Conc.}^2 * \text{NanoP}$$

Material: CN

$$\text{Oil Remov.} = +79.21226 + 0.017129\,\text{Oil Conc.} - 1.55147\,\text{NanoP} - 0.003761\,\text{Oil Conc.} * \text{NanoP} - 4.60551\text{E-06}\,\text{Oil Conc.}^2 + 2.45172\,\text{NanoP}^2 + 1.36887\text{E-06}\,\text{Oil Conc.}^2 * \text{NanoP}$$

The obtained results ranged from 83.33 to 98.61 with a ratio of 1.18, which indicated no need for power transformation of model response.

3.4.1 | Model fitting and model evaluation

The fit summary results with all factors of different models including linear, 2FL, quadratic, cubic and quartic suggested Quadratic model with an Adjusted R^2 0.8906 as presented in Table 4. Although the full Cubic model exhibited a higher Adjusted R^2 value (0.9249), its Predicted R^2 (0.3839) was substantially lower, indicating poor predictive capability and potential overfitting. Therefore, the full Cubic model was not considered suitable for prediction purposes despite its improved goodness-of-fit. In accordance with the parsimony principle, model selection was based not only on Adjusted R^2 but also on Predicted R^2, lack-of-fit statistics, hierarchy, and predictive reliability.

ANOVA results were monitored for the best model selection to find best model fit and an insignificant lack of fit (Table 5). Therefore, the modeling procedure was initiated with the Quadratic model. Subsequently, hierarchical refinement was performed by selectively incorporating statistically significant higher-order interaction terms while eliminating non-significant cubic components. This resulted in a Reduced Cubic model that preserved model hierarchy and improved predictive accuracy without introducing overfitting. It was important to fit a model with the highest significant terms while keeping the model's prediction performance high as well.

The ANOVA results and fit statistics are provided in Tables below for the best adjusted model.

The results of two runs no. 15 and no. 17 were excluded for being outliers.

The ANOVA results present the relevant statistical values for the best-fit model. The *F*-value of 36.83 indicates that the model is significant. In addition, the *p*-values listed in Table 5 show the effectiveness of each term in the equation, where a low *p*-value indicates statistical significance. For the best fit, the terms A, B, AB, A^2, and A^2B were significant, while some insignificant factors were omitted from the model. However, certain terms were retained to maintain the model hierarchy. The boundary significance level of the *p*-value was 0.1000.

The fit statistics for the modified model are presented in Table 6. The close values of predicted and adjusted R^2, 0.8919 and 0.9471

TABLE 4 Fit summary response 1: Oil Remov.

Source	Model *p*-value	Lack of fit *p*-value	Adjusted R^2	Predicted R^2	
Design Model	0.0002	0.4046	0.8862	0.5561	
Linear	0.0002	0.0999	0.6129	0.4974	
2FI	0.6367	0.0859	0.5821	0.3008	
Quadratic	**0.0001**	**0.4461**	**0.8906**	**0.7884**	**Suggested**
Cubic	0.2720	0.5754	0.9249	0.3839	
Quartic	0.5754		0.9134		Aliased

ANOVA results were examined to identify the most appropriate model and to detect any non-significant lack of fit; therefore, the modeling process was initiated with the Quadratic model

TABLE 5 ANOVA for modified quadratic model.

Source	Sum of squares	df	Mean square	F-value	*p*-value	
Model	415.32	10	41.53	36.83	< 0.0001	Significant
A-Oil Conc.	95.56	1	95.56	84.74	< 0.0001	
B-NanoP	6.11	1	6.11	5.42	0.0422	
C-Material	0.1380	1	0.1380	0.1224	0.7337	
AB	16.65	1	16.65	14.76	0.0033	
AC	0.5993	1	0.5993	0.5315	0.4827	
BC	0.9863	1	0.9863	0.8746	0.3717	
A^2	93.62	1	93.62	83.02	< 0.0001	
B^2	5.56	1	5.56	4.93	0.0507	
A^2B	13.13	1	13.13	11.64	0.0066	
B^2C	4.74	1	4.74	4.20	0.0675	
Residual	11.28	10	1.13			
Lack of Fit	5.73	7	0.8189	0.4431	0.8309	Not significant
Pure Error	5.54	3	1.85			
Cor Total	426.60	20				

TABLE 6 Fit statistics for the modified model.

Std. Dev.	1.06
Mean	91.89
C.V. %	1.16
R^2	0.9736
Adjusted R^2	0.9471
Predicted R^2	0.8919
Adeq precision	18.5553

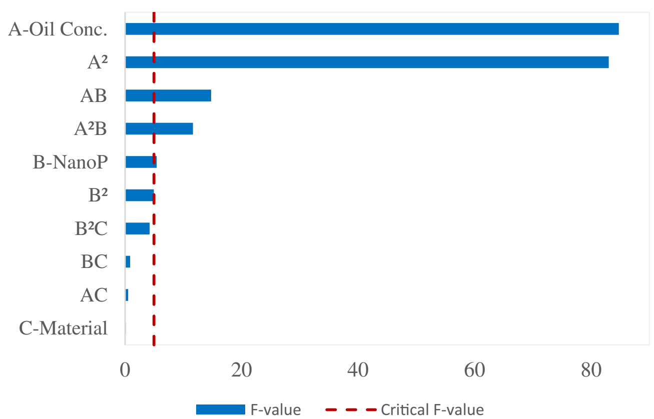

FIGURE 8 Pareto chart of the *F*-values of model terms for oil removal efficiency. The vertical line represents the critical *F*-value at the 95% confidence level ($\alpha = 0.05$). Terms exceeding the line are statistically significant.

respectively, indicate that the model is not only adequately fitted to the test data but also highly predictive. The high adequate precision value of 18.5 further shows that the signal within the variable domain is much stronger than the random error noise. Therefore, it can be concluded that the model can be used effectively for predicting new responses within the design space.

It is important to note that, unlike the full Cubic model, the Reduced Cubic model demonstrated strong predictive agreement, with a Predicted R^2 (0.8919) in close agreement with the Adjusted R^2 (0.9471). The difference between these values is less than 0.2, which confirms the absence of overfitting and indicates robust predictive capability. This validates that the selected model achieves an appropriate balance between model complexity and predictive performance.[39]

The effects of the independent variables and their interaction were evaluated using the Pareto chart. The critical *F*-value ($F_{0.05}(1, 10) = 4.96$) was determined from the *F*-distribution table based on the residual degrees of freedom.[40] The Pareto analysis (Figure 8) indicates that oil concentration (A) and its quadratic term (A^2) are the dominant contributors to oil removal efficiency, accounting for over 44% of the total model variance. Interaction and nanoparticle dosage effects are comparatively minor, while material type shows negligible statistical contribution. The interaction term AB and higher-order interaction A^2B also show statistically significant contributions. In contrast, the material type (C) and its interactions demonstrate negligible effects within the studied range. These findings indicate that process performance is primarily controlled by oil concentration and nanoparticle dosage rather than material category alone.

The plot of predicted versus actual response in Figure 9 values in the figure below shows high prediction strength of the fitted model.

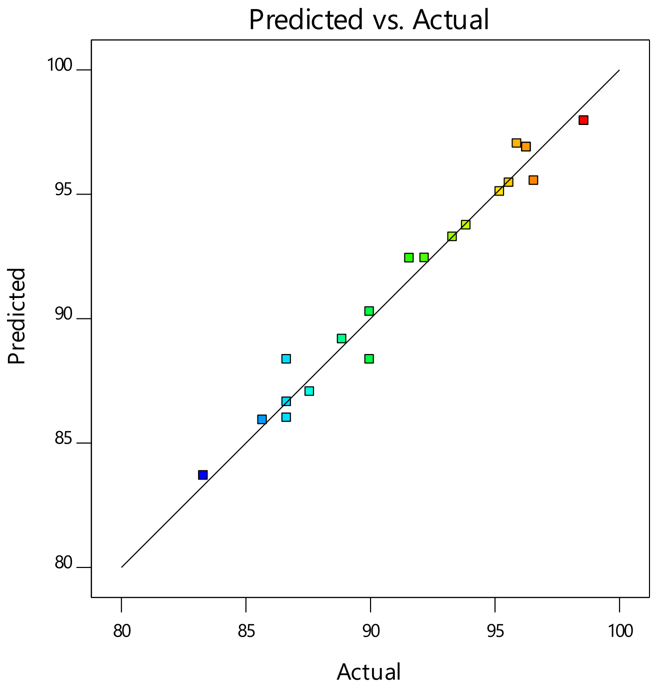

FIGURE 9 The plot of model predicted versus actual response.

3.4.2 | Discussion of the model output

The perturbation plots in Figure 10 for NC and CN show how the removal efficiency is affected by the input factors along the tested ranges. The perturbation plots are prepared for the middle value ranges of oil concentration and 1% NanoP. It shows that for NC, when the oil concentration is kept constant at 1850, adding a nanoparticle would improve the performance where the effect is also linear and proportional. In contrast, adding nanoparticles at low concentrations adversely affected CN, whereas increasing the amount of nanoparticles has significantly improved the results.

3D plots of oil removal against nanoparticle percentage and initial oil concentration in Figure 11 below represent a nonlinear behavior of the whole process. Removal efficiency was better for both materials, NC and CN, when a higher oil concentration up to ~2200 in the feed was tested. Still, this increase did not continue for higher concentrations. The addition of NC nanoparticles improved the performance throughout the oil concentration. Range, but the case for CN was interestingly different, where a low amount of NanoP enhanced the removal efficiency. Then, further addition of NanoP improved efficiency significantly, as can be seen in the figures below. Another significant observation regarding the amount of NanoP was that a high

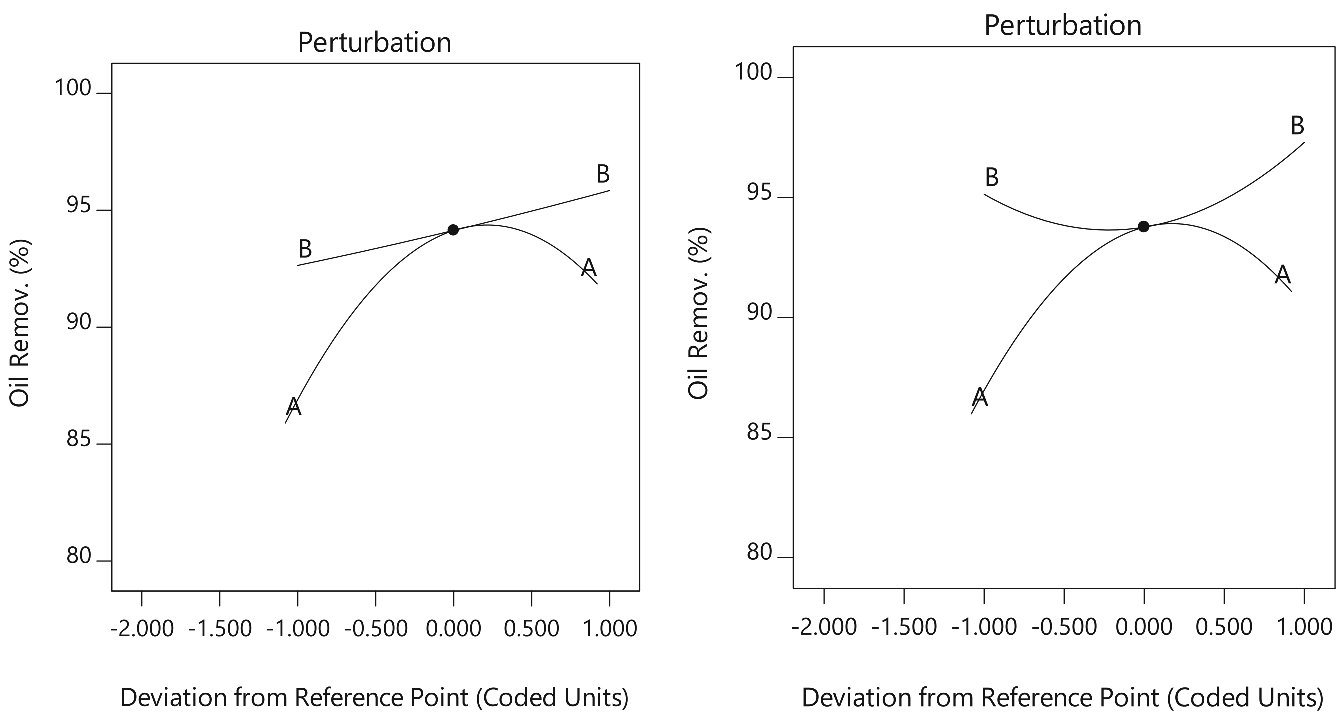

FIGURE 10 Perturbation plot for NC (left) and CN (right) at 1850 value of oil concentration and 1% Nano.

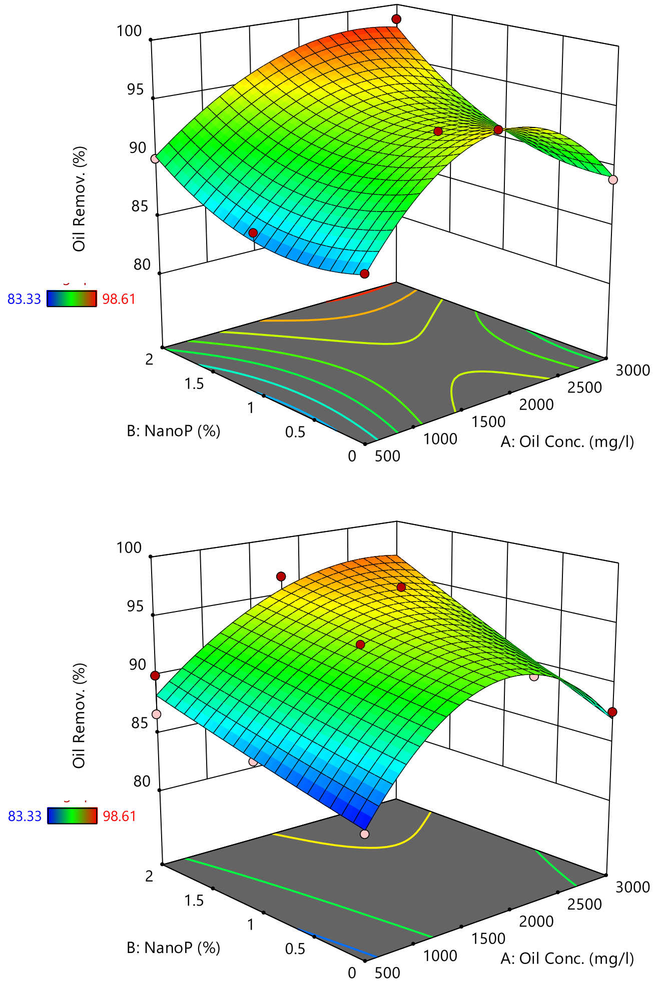

FIGURE 11 3D plot of model output vs. NanoP % (top: CN, down: NC) and oil Conc. at all ranges.

amount of Nano (%), up to 2% improved the removal efficiency performance at all ranges of oil concentration for both NC and CN.

3.4.3 | Optimization results

The obtained results when maximum removal efficiency were targeted during optimization provide multiple solutions with highest desirability in the range of input data. The range of the variables is specified in Table 7 below. The desirability of the solution based on the statistical analyses is also presented in graph (Figure 12 below) over the whole data space. Solutions for 2 combinations of categoric factor levels (NC and CN) are presented in graph below. The results show that the top ranked solution to optimize the process is an oil Conc. = 2572.73, NanoP = 2.000 and Material = CN. At this condition oil removal = 98.271% with a significantly high desirability = 0.978 can be reached.

The value for the best solutions shows that in general CN had better performance compared with NC. As listed below, the first 6 best solutions CN is suggested.

TABLE 7 (a) Constraints applied for optimization and the optimum solutions. (b) Solutions found for maximized removal efficiency.

(a)

Name	Goal	Lower limit	Upper limit	Lower weight	Upper weight	Importance
A: Oil Conc.	is in range	500	3000	1	1	3
B: NanoP	is in range	0	2	1	1	3
C: Material	is in range	NC	CN	1	1	3
Oil Remov.	maximize	83.33	98.61	1	1	3

(b)

No.	Oil Conc.	NanoP	Material	Oil Remov.	Desirability	
1	**2572.733**	**2.000**	**CN**	**98.271**	**0.978**	**Selected**
2	2559.241	2.000	CN	98.271	0.978	
3	2618.457	2.000	CN	98.267	0.978	
4	2448.915	2.000	CN	98.243	0.976	
5	2396.722	2.000	CN	98.214	0.974	
6	2006.609	2.000	CN	97.674	0.939	
7	2663.447	2.000	NC	97.078	0.900	
8	2672.867	2.000	NC	97.077	0.900	
9	2650.015	2.000	NC	97.077	0.900	
10	2683.263	2.000	NC	97.077	0.900	
11	2594.315	2.000	NC	97.069	0.899	
12	2768.748	2.000	NC	97.057	0.898	
13	2546.128	2.000	NC	97.052	0.898	
14	2394.196	2.000	NC	96.943	0.891	

Solutions found for maximized removal efficiency for CN using RSM.

Regarding the effect of initial oil concentration, the results show that handling a high concentration of 2500 is possible. The high concentration is also suggested for NC material.

Some of the set values which fall in the maximized oil removal regions on the contour graph are listed in table below.

3.5 | Comparison

Table 8 presents a clear overview of recent studies utilizing clay-based membrane additives for oil removal, demonstrating consistently high oil rejection rates (ranging from 95% to over 99.9%) across different oil types, including crude oil, lubricant oil, and vegetable oil.

The high removal efficiencies highlight the significant role of clay materials such as halloysite, montmorillonite, and nanoclays, which can significantly improve membrane performance by increasing hydrophilicity and fouling resistance. This study achieved oil removal rates of 97.08% and 98.27% with PSF/Nanoclay and PSF/Nanomer clay membranes, respectively. Results show that incorporating nanoclay into membranes is a promising approach for efficiently treating oily wastewater and matches values reported in previous research.

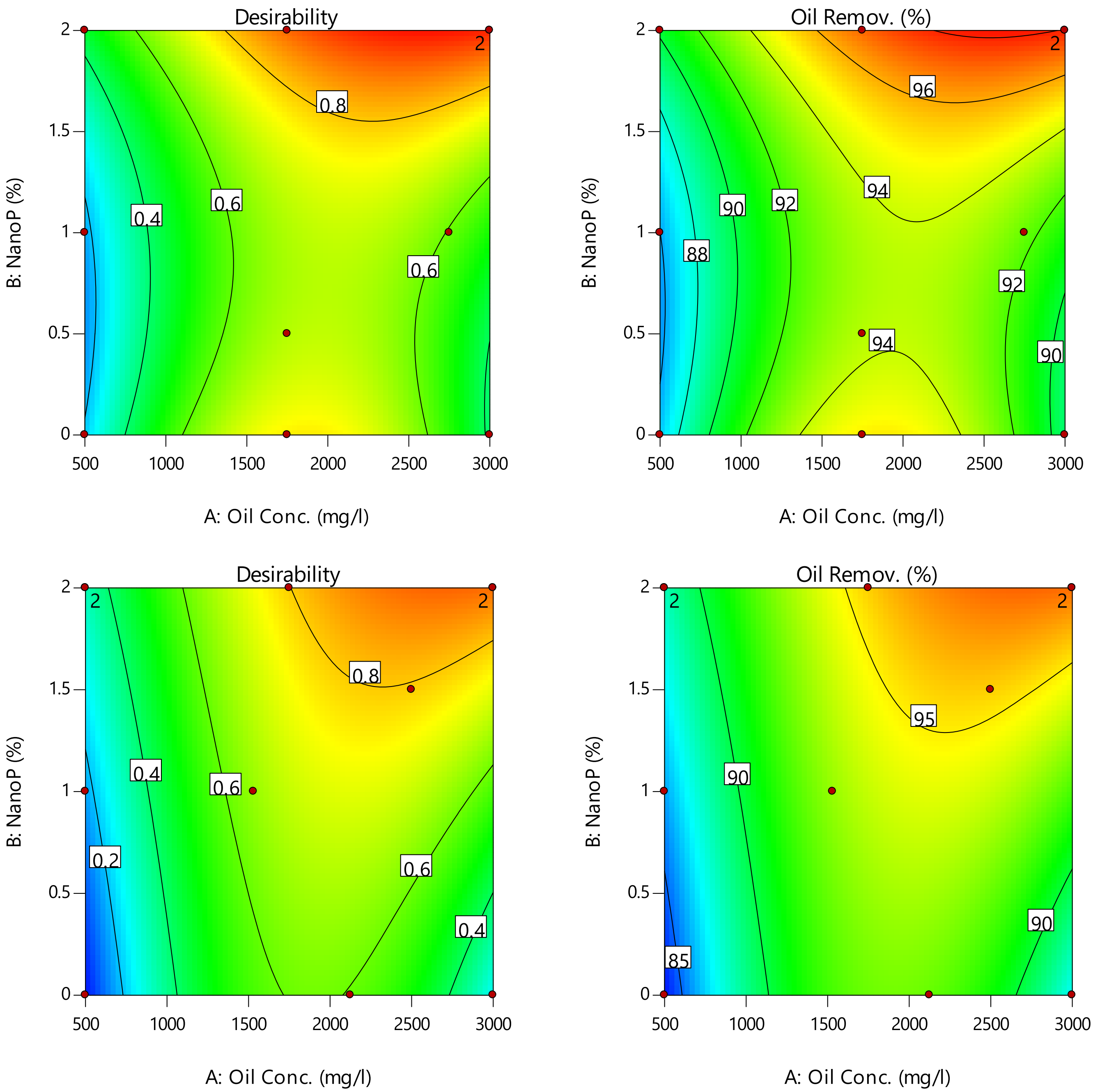

FIGURE 12 The optimization solutions at the tested data range space for oil removal efficiency and desirability plots for CN: top and NC: down.

As summarized in Table 8, while numerous studies have successfully utilized clay-based additives to achieve high oil rejection rates (typically >95%), our nanoclay-enhanced PSF membranes exhibit several distinct advantages that address existing gaps in the literature. First, most of the cited studies evaluate their membrane performance using synthetic oil-in-water emulsions or relatively low initial oil concentrations. In contrast, our optimally modified membranes maintained an outstanding rejection of over 98% even when challenged with completely real, heavy-duty waste vegetable oil at severe concentrations up to 3000 mg/L. Furthermore, beyond just separation efficiency, our membranes demonstrated exceptional antifouling resilience, achieving a Flux Recovery Ratio (FRR) of over 96%. This indicates a predominantly reversible fouling mechanism, which is often a major challenge and a limiting factor for traditional clay-modified membranes reported in the literature. Finally, by employing Response Surface Methodology (RSM), this study goes beyond a simple performance report; it provides a comprehensive statistical framework comparing commercial nanoclay (NC) with organically modified nanomer clay (CN), proving that low-cost, naturally abundant nanoclays can sustainably and economically handle complex, real-world industrial effluents.

TABLE 8 Comparison of membranes based on clay for rejection of oil.

Membrane	Additives	Type of oil	Oil rejection %	References
Tubular ceramic membrane	Ball clay/Talc/Al_2O_3	Crude oil	>99	41
Ceramic microfiltration membrane	Kaolin clay/PVA	Commercial gas-oil	~95%	42
Composite membrane	Clay/TiO_2/PVA	Crude oil	99	43
Ceramic membrane	Pozzolanik clay/Nb_2O_5/TiO_2	North Sea heavy crude oil-in-water emulsion	~98–99.5	44
Ceramic membrane	95% Clay/5% starch	Lubrax lubricant oil	99.91	45
A red clay/nano-activated carbon membrane	Red clay/CaF_2/NAC	Ultra-pure paraffin oil	>95	18
Mixed matrix membranes	Halloysite (HT) and montmorillonite (MMT)	Oily wastewater	>95	46
Composite electrospun fiber membrane	Co–polyamide/halloysite nanoclay	Vegetable oil	97	47
PSF/NC	Nanoclay	Waste vegetable oil	97.08	This study
PSF/CN	Nanomer clay		98.27	

3.6 | Economic feasibility and practical implications

From an economic feasibility perspective, the proposed PSF/NC and PSF/CN membranes offer several distinct cost advantages for potential industrial scale-up. First, the utilization of natural and commercially abundant clay-based nanoparticles (NC and CN) as membrane additives provides a highly cost-effective alternative to expensive synthetic nanomaterials typically used in literature (e.g., carbon nanotubes or complex metal oxides). Second, the significant improvements in permeability (water flux) and the high oil rejection efficiency (up to 98.27%) inherently reduce the required energy consumption (transmembrane pumping pressure) during the continuous filtration process. Furthermore, the membranes demonstrated predominantly reversible fouling; the high flux recovery ratio (FRR) achieved through a simple physical rinsing process with deionized water eliminates the need for frequent, costly, and environmentally harmful chemical cleaning agents. By integrating these low-cost natural materials with the statistical optimization framework provided by the RSM model, this study minimizes both experimental resource waste and future operational costs, strongly supporting the economic viability of the modified nanocomposite membranes for large-scale oily wastewater treatment.

3.7 | Limitations and future research directions

Although the nanoclay-enhanced membranes showed excellent oil rejection and antifouling performance, there are a few limitations to consider. Since the experiments were carried out under controlled laboratory conditions, our RSM model is specifically limited to the tested ranges (500–3000 mg/L oil and 0%–2% nanoclay). Real industrial wastewater is usually much more complex, often presenting extreme pH levels, high salinity, and various surfactants that were not included in this study. Also, our tests focused on short-term filtration, meaning the long-term continuous stability of the membranes needs further investigation.

Moving forward, future research should aim to test these membranes in pilot-scale continuous cross-flow systems using actual industrial effluents. It would also be valuable to investigate how the membrane's hydration layer holds up under harsh conditions, such as high salinity or extreme pH. Additionally, combining nanoclays with other green additives could be explored to further minimize irreversible fouling. Lastly, since economic feasibility is a major factor for industrial scale-up, conducting a techno-economic analysis (TEA) would be a highly practical next step.

4 | CONCLUSION

The incorporation of NC and CN into the polymer matrix has been demonstrated to enhance the hydrophilicity and structural stability of PSF membranes, resulting in an improvement in oil–water separation performance. The experimental results showed high agreement with the values predicted by the RSM model.

The contact angle test results confirmed that the addition of NC and CN increased the hydrophilicity of PSF membranes. When comparing PSF membranes with NC and CN additions, the higher surface wettability of those with NC additions may be explained by the strong interactions between the polymer matrix and the interface. Fundamentally, the scientific rationale behind this enhanced performance lies in the migration of the polar functional groups of the nanoclays to the membrane surface during the phase inversion process. This migration establishes a tightly bound surface hydration layer via hydrogen bonding. This stable water layer acts as a robust energetic and physical barrier exhibiting underwater oleophobicity, which strongly repels hydrophobic waste vegetable oil droplets and prevents fouling. The PSF/NC and PSF/CN clay membranes demonstrated high oil removal efficiencies of 97.08% and 98.27%, respectively.

The optimized conditions obtained using RSM have provided a valuable framework for designing high-performance membranes adapted to environmental remediation applications. The final Reduced Cubic model was selected after rejecting the full Cubic model due to overfitting concerns, as evidenced by its low Predicted R^2. The adopted model satisfies parsimony principles while maintaining high explanatory power and predictive reliability. It gives a trustworthy model capable of investigating the effect of multiple variables in the tested ranges. Application of the Reduced Cubic model could capture curvature in the response surface, which is expected in multiparametric studies with complex behavior. The cross-products in the model enable the model to predict possible interactions and the effect of parameters on each other. The model was then used to find optimized conditions for the highest removal efficiency and possible desirability.

In terms of industrial application, the high oil rejection (>98%) and flux recovery (96.2%) indicate that low-cost clay additives are a viable option for treating heavy oil loads. This approach offers a practical way to extend membrane lifespan and reduce operational costs, supporting sustainable wastewater management in the food industry. To build upon these promising findings, future research directions should focus on evaluating the long-term stability and continuous anti-fouling performance of these modified membranes in pilot-scale industrial setups using real continuous effluents. Furthermore, investigating the impact of complex wastewater chemistries (such as high salinity and various surfactants) on the surface hydration layer and exploring the potential synergistic effects of combining nanoclays with other green additives will be crucial for developing next-generation hybrid membrane systems.

AUTHOR CONTRIBUTIONS

Pınar Boyraz: Writing – original draft. **Name Nur Alibaz:** Writing – original draft. **Ayse Gul:** Writing – original draft; writing – review and editing; methodology; investigation. **Dilek Senol-Arslan:** Conceptualization; investigation; writing – original draft; writing – review and editing; methodology. **Mesut Baris:** Methodology; data curation; writing – review and editing; writing – original draft; investigation.

ACKNOWLEDGMENTS

We would like to thank Professor Dr. Niğmet Uzal for providing access to the laboratory facilities during this research.

DATA AVAILABILITY STATEMENT

The data that support the findings of this study are available from the corresponding author upon reasonable request.

ORCID

Dilek Senol-Arslan https://orcid.org/0000-0001-9639-2843
Mesut Baris https://orcid.org/0000-0002-7924-8396

REFERENCES

1. Senol-Arslan D, Gul A. Enhancing oil rejection in PVDF and PSF membranes: the role of SiO_2 NPs. *J Appl Polym Sci*. 2025;142(11):e56590. doi:10.1002/app.56590
2. Jiang J, Chen Z, Yu Z, et al. Photocatalytic composite membrane synergy contributes to efficient oil-water separation, metal ion removal and dye degradation. *Sep Purif Technol*. 2025;371:133356. doi:10.1016/j.seppur.2025.133356
3. Ghamari S, Tourani S. Development of polysulfone-based nanocomposite membranes reinforced with magnetic graphene oxide for efficient mercury and oil removal from wastewater. *Mater Sci Eng B*. 2025;317:118190. doi:10.1016/j.mseb.2025.118190
4. Achylov A, Kaygın B. Recycling of waste vegetable oils. *Bartın University Int J Nat Appl Sci*. 2022;5(2):95-100. doi:10.55930/jonas.1160433
5. Xiao Y, Xiao F, Ji W, Wang H, Li L, Wang H. A novel multifunctional Janus membrane for on-demand oil–water separation and Cr (VI) removal highly efficient. *Sep Purif Technol*. 2025;364:132588. doi:10.1016/j.seppur.2025.132588
6. Gupta R, Gupta A, George JK, Verma N. Activated carbon fabric-supported laser induced graphene-based super-hydrophobic membrane for microfiltration of water-in-oil emulsion. *Colloids Surf A Physicochem Eng Asp*. 2025;709:136085. doi:10.1016/j.colsurfa.2024.136085
7. Alseksek YK, Arumugham T, Hasan SW. Ultrafiltration membrane based on PES/CeO_2-MoS2 heterostructured nanocomposites for enhanced oil-in-water emulsion separation and antifouling. *Sep Purif Technol*. 2025;367:132921. doi:10.1016/j.seppur.2025.132921
8. Sharma R, Jain M. Removal of benzothiophenes from model diesel/jet oil fuel by using pervaporation process: estimation of mass transfer properties of the different membranes and dynamic modeling of a scale-up batch process. *J Membr Sci*. 2020;595:117500. doi:10.1016/j.memsci.2019.117500
9. Shao B, Liu Y, Jiang W, Chen N, Wang J, Li J. Experimental study on oil removal performance and anodic dissolution characteristics during the treatment of marine oil spills using electrocoagulation. *J Water Process Eng*. 2024;68:106432. doi:10.1016/j.jwpe.2024.106432
10. Wagih N, Mahmoud MM, Elbaz AA, EL-Moniry D. Oil removal from water using agricultural wastes-based adsorbents for the application in reverse osmosis desalination systems. *Desalin Water Treat*. 2023;316:335-355. doi:10.5004/dwt.2023.30200
11. Bai H, Sun Y, Tang Z, et al. Self-cleaning nanofiber membranes for sustainable dual removal of oils and dyes from wastewater. *Chem Eng J*. 2025;519:164884. doi:10.1016/j.cej.2025.164884
12. Li C, Wei W, He L, et al. Super-hydrophobic Fe/TiO_2 membrane prepared by dynamic etching of ferric salt (II) for efficient oil-water separation and photocatalytic removal of oil pollution. *J Water Process Eng*. 2024;65:105734. doi:10.1016/j.jwpe.2024.105734
13. Yin Z, Yuan F, Li M, et al. Self-cleaning, underwater writable, heat-insulated and photocatalytic cellulose membrane for high-efficient oil/water separation and removal of hazardous organic pollutants. *Prog Org Coat*. 2021;157:106311. doi:10.1016/j.porgcoat.2021.106311
14. Qu N, Chen L, Huo L, et al. The microbe-loaded silica hollow spheres doped PVDF membrane prepared by green solvent casting method for efficient oil-water separation. *Surf Interfaces*. 2025;61:106085. doi:10.1016/j.surfin.2025.106085
15. Ahmed AM, Hosny R, Mubarak MF, Younes AA, Farag AB. Green magnetic clay nanocomposite based on graphene oxide nanosheet as a synthetic low-cost adsorbent for oil droplets removal from produced water. *Desalin Water Treat*. 2022;280:206-223. doi:10.5004/dwt.2022.29031
16. Abuhasel K, Kchaou M, Alquraish M, Munusamy Y, Jeng YT. Oily wastewater treatment: overview of conventional and modern methods, challenges, and future opportunities. *Water*. 2021;13(7):980. doi:10.3390/w13070980
17. Arbelaiz A, Fernández G, Orue A. The effect of montmorillonite modification and the use of coupling agent on mechanical properties of polypropylene–clay nanocomposites. *Polym Polym Compos*. 2021;29(6):660-671. doi:10.1177/0967391120930613

18. Aljlil SA. Development of red clay ultrafiltration membranes for oil-water separation. *Crystals*. 2021;11(3):248. doi:10.3390/cryst11030248
19. Nandi, B. K., Uppaluri, R., & Purkait, MKTreatment of Oily Waste Water Using Low-Cost Ceramic Membrane: Flux Decline Mechanism and Economic Feasibility. *Separation Science and Technology*, 2009; 44 (12), 2840–2869. doi:10.1080/01496390903136004
20. Vasanth D, Pugazhenthi G, Uppaluri R. Cross-flow microfiltration of oil-in-water emulsions using low cost ceramic membranes. *Desalination*. 2013;320:86-95. doi:10.1016/j.desal.2013.04.018
21. Aloulou W, Aloulou H, Amar RB. Low-cost composite ultrafiltration membrane made from TiO_2 and nanocomposite clay materials over zeolite support for oily wastewater purification and heavy metals removal. *Desalin Water Treat*. 2022;246:166-173. doi:10.5004/dwt.2022.28027
22. Choe E, Min DB. Chemistry of deep-fat frying oils. *J Food Sci*. 2007; 72(5) R77–R86. doi:10.1111/j.1750-3841.2007.00352.x
23. Zulaikha S, Lau WJ, Ismail AF, Jaafar J. Treatment of restaurant wastewater using ultrafiltration and nanofiltration membranes. *J Water Process Eng*. 2014;2:58-62. doi:10.1016/j.jwpe.2014.05.001
24. Ferdowsi A, Kikhavani T, Ashrafizadeh SN. Enhancement in performance of the PVC/Nanoclay mixed matrix Nanofiltration membrane. 2022. doi:10.21203/rs.3.rs-1741723/v1
25. Vahedi M, Sherafat Z, Bagherzadeh E. Improved water flux in optimized electrospun polysulfone/nanoclay membranes. *Polym Compos*. 2022;43(5):2602-2614. doi:10.1002/pc.26560
26. Ma Y, Shi F, Zhao W, et al. Preparation and characterization of PSf/clay nanocomposite membranes with LiCl as a pore forming additive. *Desalination*. 2012;303:39-47. doi:10.1016/j.desal.2012.07.016
27. El Moustansiri H, El Abbadi S, Douma M, et al. Development of low-cost wollastonite based-membrane from clay for efficient microfiltration of textile and tannery wastewaters. *Sep Purif Technol*. 2025;359: 130770. doi:10.1016/j.seppur.2024.130770
28. Arslan DS, Hacifazlioglu H. Performance comparison of waste cooking oil on coal slime flotation with sunflower oil and gas oil. *Hittite J Sci Eng*. 2023;10(4):337. doi:10.17350/HJSE19030000323
29. Gui X, Xing Y, Wang T, Cao Y, Miao Z, Xu M. Intensification mechanism of oxidized coal flotation by using oxygen-containing collector α-furanacrylic acid. *Powder Technol*. 2017;305:109-116. doi:10.1016/j.powtec.2016.09.058
30. Wang J, Sun H, Gao X, Gao C. Enhancing antibiofouling performance of Polysulfone (PSf) membrane by photo-grafting of capsaicin derivative and acrylic acid. *Appl Surf Sci*. 2014;317:210-219. doi:10.1016/j.apsusc.2014.08.102
31. Rodrigues R, Morihama ACD, Barbosa IM, Leocádio GN, Mierzwa JC. Clay nanoparticles composite membranes prepared with three different polymers: performance evaluation. *J Membr Separ Technol*. 2018; 7:1-11. doi:10.6000/1929-6037.2018.07.01
32. Ma Y, Shi F, Wang Z, Wu M, Ma J, Gao C. Preparation and characterization of PSf/clay nanocomposite membranes with PEG 400 as a pore forming additive. *Desalination*. 2012;286:131-137. doi:10.1016/j.desal.2011.10.040
33. Karbol MS, Al-Jubouri S. Oily water treatment by polyacrylonitrile/polysulfone blend ultrafiltration membrane embedded with alumina nanoparticles of improved antifouling properties. *Global NEST J*. 2025;1–12. doi:10.30955/gnj.07817
34. Saki S, Senol-Arslan D, Uzal N. Fabrication and characterization of silane-functionalized Na-bentonite polysulfone/polyethylenimine nanocomposite membranes for dye removal. *J Appl Polym Sci*. 2020; 137(36). doi:10.1002/app.49057
35. Huang S, Ras RHA, Tian X. Antifouling membranes for oily wastewater treatment: interplay between wetting and membrane fouling. *Curr Opin Colloid Interface Sci*. 2018;36:90-109. doi:10.1016/j.cocis.2018.02.002
36. Obaid M, Alsadun N, Shekhah O, et al. Deployment of Superhydrophilic and super-antifouling Cr- soc -MOF-1-based membrane for ultrafast separation of stabilized oil-in-water emulsions. *ACS Appl Mater Interfaces*. 2023;15(25):31067-31076. doi:10.1021/acsami.3c05285
37. Ahmad NA, Goh PS, Abdul Karim Z, Ismail AF. Thin film composite membrane for oily waste water treatment: recent advances and challenges. *Membranes*. 2018;8(4):86. doi:10.3390/membranes8040086
38. Rani SLS, Satyannarayana KVV, Arthanareeswaran G, Raja VK. Treatment of food processing industries wastewaters using a new clay-based inorganic membrane: performance evaluation and fouling analysis. *J Taiwan Inst Chem Eng*. 2025;166:105439. doi:10.1016/j.jtice.2024.105439
39. Shakor ZM, AbdulRazak AA, Shuhaib AA. Optimization of process variables for hydrogenation of cinnamaldehyde to cinnamyl alcohol over a Pt/SiO_2 catalyst using response surface methodology. *Chem Eng Commun*. 2022;209(6):827-843. doi:10.1080/00986445.2021.1922394
40. Sarran MA, AbdulRazak AA, Abid MF, Jawad AD. Oily wastewater treatment using low-cost and highly efficient natural and activated Iraqi bentonite. *Desalin Water Treat*. 2024;319:100412. doi:10.1016/j.dwt.2024.100412
41. de Souza MYM, Lira H d L, Santana LN d L, Rodríguez MA. Preparation and application in crude oil-water separation of clay-based membranes. *Mater Res*. 2021;24(4):e20200508. doi:10.1590/1980-5373-mr-2020-0508
42. Sheikhi M, Arzani M, Mahdavi HR, Mohammadi T. Kaolinitic clay-based ceramic microfiltration membrane for oily wastewater treatment: assessment of coagulant addition. *Ceram Int*. 2019;45(14): 17826-17836. doi:10.1016/j.ceramint.2019.05.354
43. Suresh K, Pugazhenthi G. Cross flow microfiltration of oil-water emulsions using clay based ceramic membrane support and TiO_2 composite membrane. *Egypt J Pet*. 2017;26(3):679-694. doi:10.1016/j.ejpe.2016.10.007
44. Lesak GVG, Xavier LA, de Oliveira TV, et al. Enhancement of pozzolanic clay ceramic membrane properties by niobium pentoxide and titanium dioxide addition: characterization and application in oil-in-water emulsion microfiltration. *J Pet Sci Eng*. 2022;217:110892. doi:10.1016/j.petrol.2022.110892
45. dos Santos Barbosa A, dos Santos Barbosa A, Rodrigues MGF. Low cost membrane used in oil/water removal. *Desalin Water Treat*. 2024; 317:100029. doi:10.1016/j.dwt.2024.100029
46. Yogarathinam LT, Ismail AF, Arthanareeswaran G, Azali MAB, Ramli MKNB, Rushdan A. Impact of Nanoclays on Polyvinylidene fluoride mixed matrix membranes for the efficient treatment of oily wastewater. *Micro Nanosyst*. 2023;15(1):35-42. doi:10.2174/1876402914666220622095858
47. Bhagyaraj S, Sobolčiak P, Al-Ghouti MA, Krupa I. Copolyamide–clay nanotube polymer composite nanofiber membranes: preparation, characterization and its asymmetric wettability driven oil/water emulsion separation towards sewage remediation. *Polymers*. 2021;13(21): 3710. doi:10.3390/polym13213710

How to cite this article: Gul A, Senol-Arslan D, Baris M, Boyraz P, Alibaz NN. Optimizing nanoclay-enhanced membranes for oil rejection using response surface methodology. *Environ Prog Sustainable Energy*. 2026;e70475. doi:10.1002/ep.70475